Pharm Res (2014) 31:1390–1406
DOI 10.1007/s11095-013-1277-z

EXPERT REVIEW

Theranostic Nanoparticles for Cancer and Cardiovascular Applications

Dan Wang • Bingbing Lin • Hua Ai

Received: 1 August 2013 / Accepted: 31 December 2013 / Published online: 5 March 2014

ABSTRACT Theranostics have received enormous attentions for individualized diagnosis and treatment in the past few years. Especially, the availability of various nanoplatforms provides great potentials for designing of sophisticated theranostic agents including imaging, targeting and therapeutic functions. Numerous reports have been published on how to construct multifunctional nanoparticles for the targeted diagnosis and therapy simultaneously since the concept of "theranostics". This review presents recent advances of molecular imaging and nanoplatform technology, and their applications in drug discovery and development. Applications of nanoplatform-based theranostics in cancer and cardiovascular diseases will also be covered including diagnosis, assessment of drug biodistribution, and visualization of drug release from nanoparticles, as well as monitoring of therapeutic effects.

KEYWORDS Drug delivery · Nanoplatforms · Theranostics · Cancer · Cardiovascular diseases

INTRODUCTION

With the growing trend towards the advancement of personalized medicine, theranostics used for individualized diagnosis and treatment has received enormous attentions in recent years (1–4). Theranostic entities simultaneously deliver imaging agents and therapeutic drugs within the same dose, and enable one to monitor pathological sites, delivery kinetics, drug distribution and release, as well as therapeutic efficacy. Based on these advanced capabilities, it is feasible for physicians to choose individualized medicine and make effective decisions in real-time, such as choice of treatment type, procedure, and quantity of a drug (5). In order to reach an effective drug concentration at a site of interest, the multifunctional entity can be endowed with a targeting moiety to achieve site-specific therapy and imaging (6). The potential benefits of theranostics for patients are maximization of therapeutic effects with minimized adverse events in conventional systemic administrations (7). Besides, the combined technique promotes the development of new drugs, even no theranostic drug has been approved by U.S. Food and Drug Administration (FDA).

The availability of various nanoplatforms provides the opportunities for better drug carrier design with imaging functionality (8,9). Clinically relevant nanoplatforms include polymer-drug conjugates, polymer micelles, liposomes, and dendrimers, etc. These nanoplatforms can conjugate or entrap drugs and offer a number of advantages over conventional formulations in certain applications (8). Due to nanosize, nanoplatforms can prolong the circulation time of the drug, selectively deliver anticancer drugs to tumor tissues by passive or active targeting, and control drug release by delivery systems responsive to a stimulus such as pH, temperature, light, ultrasound, or enzyme degradation, leading to a desired drug release rate and concentration at the site of action (10). Additionally, one important advantage of nanoplatforms is that they can integrate diagnostic and therapeutic components with targeting moieties (11,12). Even at their early stages of development, the field of nanoplatform-based theranostics is growing exponentially thanks to advances in nanotechnology and the call for personalized medicine.

With technological advances in instrument performance and the toolbox for imaging reconstruction software, molecular imaging has become an indispensable tool in preclinical research and clinical trials, including magnetic resonance imaging (MRI), computed tomography (CT), optical imaging, ultrasound (US) imaging, positron emission tomography

D. Wang • B. Lin • H. Ai (✉)
National Engineering Research Center for Biomaterials
Sichuan University Chengdu 610064, People's Republic of China
e-mail: huaai@scu.edu.cn

H. Ai
Department of Radiology, West China Hospital Sichuan University
Chengdu 610041, China

(PET), and single photon emission computed tomography (SPECT). With the help of molecular probes, these imaging technologies improve their sensitivity and specificity, for better evaluation of therapeutic efficacy during drug development pathway (13–15). Incorporation of imaging probes into theranostic agents will enhance the performance of multifunctional entities. Among these options, choosing of right imaging modality is crucial in designing and optimizing of nanoplatform-based theranostic agents (16), depending on specific applications. Ideally, molecular imaging technology should enable one to study an intact living subject with excellent spatial and temporal resolution for monitoring biological processes at molecular and cellular levels, as well as with potential for sequential, longitudinal monitoring.

In this review, we will discuss the key advances in medical imaging and nanotechnology related to theranostics. In particular, we will focus on nanoplatform-based theranostic systems for diagnosis and treatinf of diseases, and discuss their applications for tracing drug delivery and monitoring of therapy, especially in the areas of cancer and cardiovascular diseases.

IMAGING MODALITY

Each imaging modality aforementioned has its own advantages and disadvantages in terms of sensitivity, spatial resolution, target, and penetration depth (Table 1). Ultrasound imaging is safe and relatively low cost, but its spatial resolution is poor comparing to CT and MRI. CT is a classical anatomical imaging modality and can deal with the visualization of organs or tissues, such as lung structures. MRI offers sensitive detection of soft tissue pathologies and conveys valuable information related to physiological process. Nuclear imaging (such as PET or SPECT) is a sensitive tool for diagnosing diseases at early stage, analyzing drug biodistribution and assessing the efficacy in living subjects, but the spatial resolution of PET is much behind ultrasound, CT and MRI. Optical imaging technology including fluorescence and bioluminescence imaging are highly sensitive, but only accessible at limited depths of a few millimeters. Combination of two or more imaging modalities may thus improve the overall function of monitoring of diagnosis and therapy.

In clinical practice, these imaging technologies are routinely implemented for early diagnosis of diseases, particularly in oncology and cardiovascular diseases, selection of personalized regimen, and monitoring of therapy efficacy. These imaging technologies have gradually become an important tool in the process of drug discovery and development for improving the efficiency of drug screening in preclinical studies, investigation of the pharmacodynamics in clinical trials (18–20). Not only do such strategies reduce the cost and workload, but also speed up drug development. It is useful to apply imaging technologies in different phases of drug development (Fig. 1), with the goal of optimizing the process and bringing drugs to the market much faster.

Among all imaging modalities, PET and SPECT imaging modalities have attracted great attention mainly due to its excellent sensitivity with low background noise. In addition, PET imaging agents, such as radioisotopes ^{11}C, ^{18}F and ^{15}O, can label drugs or targets, and keep physiochemical characteristics of the drug unchanged if not to affect their pharmacophore. Heavy-metal isotopes such as ^{64}Cu, ^{68}Ga, ^{99}mTc and ^{111}In are commonly used to label various monoclonal antibodies or peptides through chelating ligands such as DOTA (1, 4, 7, 10-tetraazacyclododecane-1, 4, 7, 10-tetraacetic acid) or TETA (1, 4, 8, 11-tetraazacyclotetradecane-1, 4, 8, 11-tetraacetic acid). The bioconjugation chemistry enables one to develop new PET or SPECT imaging probes which can be used in early drug development for accurately measuring the biodistribution and pharmacokinetics of new agents in clinical applications by quantitative PET or SPECT imaging. For example, ^{64}Cu-labeled Abegrin™ may be used for preclinical research and characterization of pharmacokinetics, treatment monitoring and dose optimization (21). In another example, Niu *et al.* studied the delivery and distribution of Cu-labeled antibodies (^{64}Cu-DOTA-cetuximab) in head and neck squamous cell carcinoma of the mice, and evaluated tumor response after ^{64}Cu-DOTA-cetuximab treatment using Fludeoxyglucose ^{18}F (FDG) PET imaging (22).

The application of molecular imaging may accelerate drug development process, while simultaneously improve the design of imaging probe and fusion imaging with molecular and anatomical imaging tools. FDG is the most widely used tracer for PET imaging in oncology by determining abnormal glucose metabolism in pathological sites to assist in diagnosing early diseases for initial staging, studying of tumor cell proliferation and metastasis, and assessment of response to chemotherapy or radiotherapy in many tumors including lymphoma, breast cancer, colorectal cancer and non-small-cell lung cancer (23–25). In 2012, the FDA approved florbetapir ^{18}F injection (Amyvid™), as a radioactive diagnostic agent for use with PET imaging, to evaluate beta-amyloid neuritic plaque density in patients who suffered from Alzheimer's Disease (AD) or other cognitive decline (26).

However, PET or SPECT imaging for pharmacokinetic studies has its limitations, such as short half-life of isotope limits time window for pharmacokinetic studies, and low spatial resolution with unsatisfactory anatomical information. With the improvement of imaging agents and instruments, these problems have been solved partially. ^{125}I is a low-energy gamma emitter, and it can image and quantify in small animals with relatively high resolution and sensitivity. Moreover, its half-life is around 59 days that can be used to evaluate the pharmacokinetic characteristics and disease

Table I Comparison of Some Key Imaging Modalities (14, 17)

Modality	Sensitivity (M)	Spatial resolution	Depth	Time	Target*	Imaging agents
MRI	10^{-3} to 10^{-5}	25–100 μm	No limit	Min-hr	A, P, M	Paramagnetic: Gd, Mn chelates Superparamagnetic: Fe_3O_4, gamma-Fe_2O_3
CT	Not well characterized	50–200 μm	No limit	Sec-min	A, P	Iodine
PET	10^{-11} to 10^{-12}	1–2 mm	No limit	Min	P, M	^{18}F, ^{11}C, ^{15}O
SPECT	10^{-10} to 10^{-11}	0.5–1 mm	No limit	Min	P, M	^{99m}Tc, ^{111}In chelates
US	Not well characterized	50–500 μm	mm-cm	Sec-min	A, P	Microbubbles
Optical imaging	Bioluminescence: 10^{-10} to 10^{-11} Fluorescence: 10^{-9} to 10^{-12}	1–3 mm	mm	Sec-min	P, M	Bioluminescence: Luciferin Fluorescence: a) dyes b) quantum dots

*: A, anatomical; P, physiological; M, molecular

response in long-term therapy (27). What's more, dual imaging modalities such as PET/CT, SPECT/CT or PET/MRI can compensate the disadvantages of each other and allow for co-registration of high resolution anatomical data with highly sensitive molecular information (28,29). Compared to PET/CT and SPECT/CT imaging, PET/MRI provides advantages in acquiring better contrast of soft tissues with excellent sensitivity (Fig. 2) (30–32).

Among all clinical imaging techniques, MRI presents unqiue value at every stage in drug discovery and development process, including in early stage for drug candidate screening, and in late stage for investigation of safety, pharmacokinetic, pharmacodynamic, and efficacy profile of a drug candidate (33). In addition, MRI provides an opportunity to bridge up the gap between preclinical and clinical studies by examining the mechanisms of drug action of candidate compounds (34).

Gadolinium (Gd) or manganese (Mn) based small paramagnetic molecules, and superparamagnetic iron oxide (SPIO) based nanoparticles, are two major categories of MRI contrast agent approved for clinical applications. Gd^{3+} and Mn^{2+} like heavy-metal isotopes coupled to chelating ligands are liable to react with the active group of drugs and targets for MRI imaging. For example, Kalber *et al.* synthesized a Gd^{3+} labeled derivative of colchicine and allowed for *in vivo* imaging of central necrosis response to colchicine therapy in ovarian carcinoma xenografts (35). SPIO nanoparticles' surface can be modified to add a wide range of functionalities, such as targeting, imaging and therapeutic groups (Fig. 3). This versatility makes the contrast-enhanced MRI imaging increasingly important in the construction of theranostic agents with many excellent examples (36,37). Besides,many fluorinated drugs or contrast agents, such as 5-Fluorouracil, perfluorocarbon (PFC)-based nanoparticles, can be used for fluorine (^{19}F) MRI and/or MR spectroscopy (MRS). Based on these imaging modalities, one is able to investigate agents' pharmacokinetics, map tumor oxygenation, assess molecular expression in vascular diseases, and visualize and/or quantify of endogenous macrophages, injected immune cells and stem cell transplants (38–43). In combination with anatomical ^{1}H MRI, ^{19}F MRI can obtain anatomical information. With further introduction of new pulse sequences and contrast agents, MRI will continue to be a powerful tool in drug discovery process, early diagnosis and assessment therapeutic efficacy in clinical applications.

NANOPLATFORM

Following the brief introduction of imaging technology and their applications in theranostic applications, we will focus here on nanoplatforms with the capability to serve as image-guided targeting drug delivery vectors. These nanoplatforms listed below are made from biocompatible polymer materials, either soluble or colloidal aqueous, and generally vary in size from 10 to 100 nm. The drug or imaging agent is either encapsulated in the core of nanocomposites or attached to the surface of nanoplatforms. Meanwhile, targeting delivery

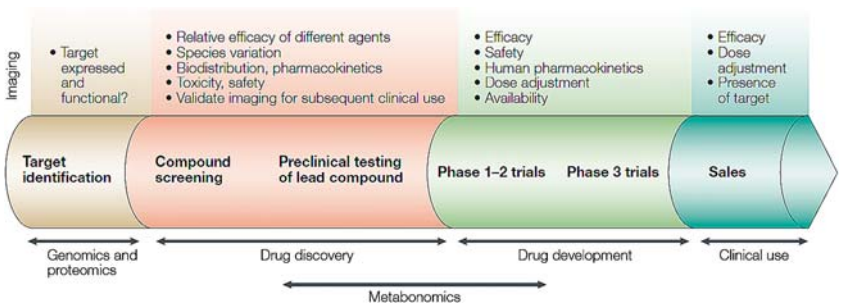

Fig. 1 Imaging application in drug discovery and development process. Images adapted with permission from ref (19)

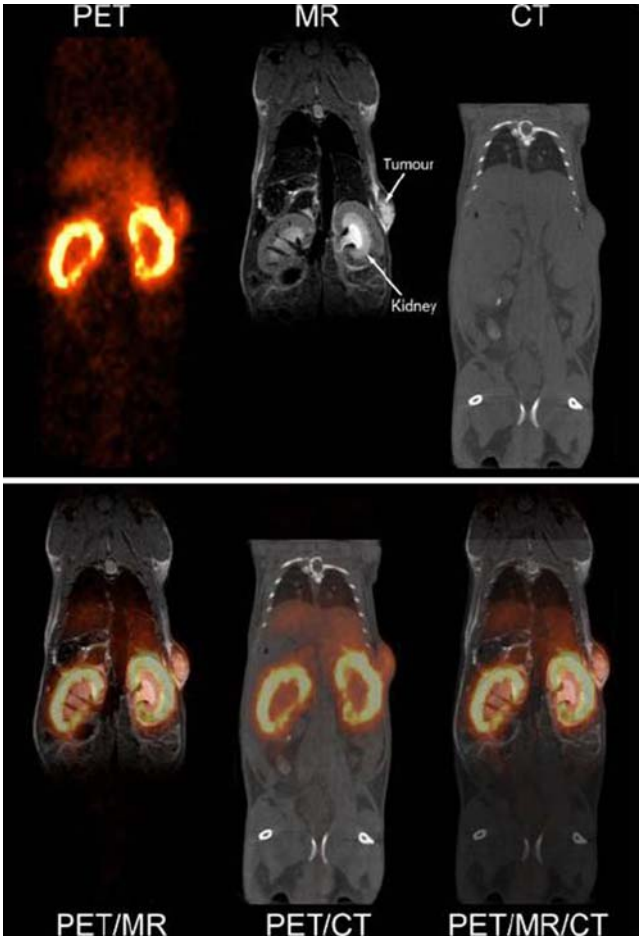

Fig. 2 *Top* PET, MR, and CT single-modality imaging with a ^{64}Cu labelled monoclonal antibody. Compared to the CT image, the PET image depicts more intuitive antibody clearance through the kidneys and the uptake in the tumour. Meanwhile, the MR image shows more excellent soft tissue contrast, and a clearer delineation between the tumour tissue and the connective tissue. *Bottom* PET/MR, PET/CT, and PET/MR/CT images show the advantage of PET/MR over PET/CT. Images adapted with permission from ref (32)

system based on nanoplateforms can be achieved by conjugation of targeting ligands on their surfaces for specific recognition of a site on diseased region. In this section, we present some excellent examples in the field of biocompatible nanoplatforms used as theranostic systems.

Drug-Conjugates and Complexes

Polymer-drug conjugation is a successful strategy in drug delivery. Conjugation of hydrophobic low-molecular-weight drugs to water-soluble polymers can improve their solubility and efficacy through passive or active targeting with reduced *in vivo* toxicity. While biomacromolecular drugs such as monoclonal antibodies or recombinant DNA can be conjugated to water-soluble polymers mainly for reduced immunogenicity, prolonged plasma half-life and enhanced stability (44,45). Conjugated drugs can be triggered to release at certain environment when the conjugation linker is responsive to extracellular or intracellular biological or chemical stimuli (46,47).

It is crucial to choose water-soluble polymer carriers that their physico-chemical properties determine biodistribution, elimination and metabolism of the conjugate as a whole. The ideal polymer carrier should be non-reactive in blood, non-toxic, non-immunogenic, and with suitable loading capacity. Some representative polymers used in clinical applications are polyethylene glycol (PEG), N-(2-hydroxypropyl)methacrylamide (HPMA) copolymers and polyglutamic acid (PGA). PEG is a particularly attractive polymer for drug conjugation, and approved by the FDA as a drug excipient in pharmaceuticals, including topical, injectable, nasal and rectal formulations. For example, therapeutic protein PEGylation has led to the development of numerous drugs, many of them have been approved and entered the market, such as PEG-asparaginase (Oncaspar®), PEG-α-

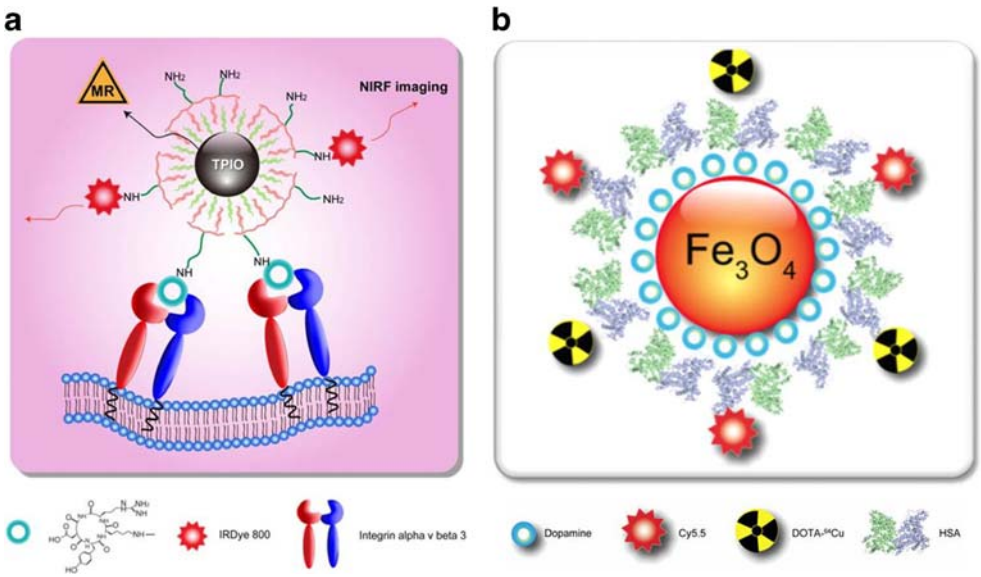

Fig. 3 Iron oxide nanoparticles coated with (**a**) a triblock copolymer and (**b**) dopamine-plus-human serum albumin to confer water solubility and functional extendibility. Images adapted with permission from refs (37)

interferon 2a (Peg-asys), PEG-α-interferon 2b (Peg-Intron) and PEG-granulocyte colony-stimulating factor (Neulasta™), etc. (48,49). However, the linear PEG can only carry one or two drug molecules via coupling to the end chains, resulting in low loading capability for delivery of small-molecular-weight drugs (50). In an effort to overcome the limitation, branched PEG and hyperbranched polymers are also being explored (44,51). In one case, Pasut group synthesized branched PEG that based on amino adipic acid or beta-glutamic acid, as branching molecules, and the large polycyclic drug epirubicin molecule was chosen to bind to polymeric carriers with high drug carrying capacity (52). Due to the hydrophobic nature of the drug and high drug loading capacity, the PEG-epirubicin conjugates tend to form micelle like aggregates, and exhibit long blood residence time which is favorable for therapeutic application. In addition, PGA can theoretically carry one drug molecule per monomer unit and display a higher loading capacity that reaches 37 wt.% PGA-Paclitaxel (53).

Importantly, polymer-drug conjugates in combination with molecular imaging technology have been widely used to investigate the mechanism of drug delivery with polymers, and monitor pharmacokinetics, biodistribution and drug targeting efficiency (54,55). Lammers *et al.* synthesized gadolinium-labeled HPMA copolymer incorporating doxorubicin and gemcitabine to analyze the biodistribution of nanotheranostics using MRI (56). The successful preclinical application of polymer-drug conjugations containing imaging modality bodes well for future design of optimized formulations.

Polymeric Micelles

Polymeric micelles, which consist of amphiphilic block copolymers that self-assemble to form core-shell architecture in water ranging from 10 to 100 nm in size. Wherein, the hydrophobic core can load water-insoluble drugs and imaging agents by physical entrapment, while the hydrophilic surface layer stabilize the micellar structure in aqueous environment, and protect nanoparticles from rapid renal exclusion and uptake by reticulo-endothelial system (RES), also, covalently bind hydrophilic imaging agents (57). Polymer micelles have been successfully used as pharmaceutical carriers for water-insoluble drugs, usually, choosing PEG as the hydrophilic shell-forming block. An example of polymeric micelles under clinical evaluation is NK105, a PEG-polyaspartic acid micelle loaded with paclitaxel, now is evaluated for breast cancer therapy in clinical phase III in Japan (www.clinicaltrials.gov/). Another polymeric micelle (PEG-PLA) entrapped paclitaxel (Genexol-PM) has been approved for clinical use for breast cancer in Korea in 2007 (Samyang Genex Co.), Phase II for pancreatic cancer, bladder cancer, and other cancers in the US (www.clinicaltrials.gov/). The study in phase I determined that the maximum tolerated dosage (MTD) of Genexol-PM was 390 mg/m^2 and 300 mg/m^2 as the recommended dose (58). The study in phase II displayed that Genexol-PM was effective and safe with high response rates (58.5%) in patients suffering from metastatic breast cancer, but caused hypersensitivity reactions in 19.5% patients in the absence of premedications (59).

Choosing biodegradable polymers as hydrophobic segment can control the release of drug payload in the core through diffusion, polymer degradation or micelle dissociation mechanisms (60,61). Besides, researchers explored different types of micelles to control drug release at target site, especially, environmentally-sensitive polymeric micellar systems (62,63). Chemical fixation of micelles by crosslinking of either the core or corona using stimuli-responsiveness ligands are developed to prepare long-circulating and sustained-release micelles (64–66). Cheng *et al.* reported an adaptable drug carrier made of disulfide bonded mPEG-$(Cys)_4$-PDLLA micelles (67). These micelles can stably retain doxorubicin in the blood stream and efficiently deliver the drug to the tumor with a 7-fold increase of the drug amount, comparing to non-crosslinked mPEG-PDLLA micelles.

Polymer micelles are thoroughly tested as imaging probes or theranostic carriers. Self-assembly of amphiphilic block copolymers can entrap the hydrophobic SPIO or Mn-SPIO nanoparticles to form clusters using for MR imaging (37,68–70). In one approach, we have designed an amphiphilic starlike polysaccharide with multi-arms of dextran linked to a β-cyclodextrin (β-CD) core through click chemistry, and it was used for encapsulation of multiple hydrophobic SPIO nanoparticles and small molecule anticancer drug doxorubicin to form a multifunctional probe (70). The probe has a T_2 relaxivity of 436.8 Fe mM^{-1} s^{-1} and is internalized into the cytoplasm of multidrug-resistant breast cancer cell line (MCF-7/Adr) after 24 h labeling. One should notice that the aggregation degree of nanoparticle are related to different values of T_2 relaxivity, higher aggregation degree usually leads to a better signal contrast enhancement. Taking alkyl-PEI2k/SPIO nanocomposite as an example, at the magnetic field of 1.5 T, T_2 relaxivity of multiple SPIO nanocrystals micelles around 79 nm is 323 Fe mM^{-1} s^{-1}, which is much higher than that of single SPIO nanocrystal containing micelles with a diameter about 12 nm (118 Fe mM^{-1} s^{-1}) (71).

Not only for entrapment of hydrophobic imaging components, polymer micelles can also be used for conjugation of chelating moieties and providing high-affinity binding of a wide range of non-radioactive or radioactive heavy metal ions, such as ^{111}In, ^{99m}Tc, ^{68}Gd, ^{67}Ga, etc., for either T_1 MR, PET or SPECT imaging. Hoang *et al.* monitored the pharmacokinetics of elimination from the blood and biodistribution of an ^{111}Indium-labeled (^{111}In) amphiphilic diblock copolymer micelle using microSPECT/CT imaging (72). The accumulation of ^{111}In-micelles in spleen, liver, and tumor at 48 h p.i. in athymic mice bearing MDA-MB-231 breast cancer

xenografts are shown in Fig. 4a and b. ^{111}In-micelles have longer circulation time up to 48 h p.i. and exhibited significantly great tumor accumulation (9±2% i.d./g). As shown in Fig. 4c, ^{111}In-micelles exhibited incomplete and nonhomogeneous distribution within the tumor nodule, with the majority located at the periphery on the transverse slices.

Quantum dots (QD) and hydrophobic fluorescent dyes are widely used as fluorescent probes for *in vitro* and *in vivo* imaging applications (73–75), but their poor biocompatibility limits their applications. Block copolymer micelles temporarily addressed this problem by wrapping hydrophobic nanocrystals and small molecules inside of them (76). The soluble fluorescent dye can be conjugated to the hydrophilic segment of micelles by chemical conjugation (77). Recently, we have synthesized amphiphilic polyethylenimine (PEI) 25 kD modified with near-infrared (NIR) fluorescent dye Cy5.5, and they were used for encapsulation of multiple hydrophobic SPIO nanoparticles to form a multimodality probe for cell labeling (78).

Multifunctional polymeric micelles with targeting capability for anticancer drug delivery and imaging of distribution have been developed, with focus on design of well controlled nanostructures. Nasongkla *et al.* constructed combinatorial polymeric micelles encapsulated therapeutic drugs doxorubicin for treatment of cancer, and co-loaded SPIO nanoparticles for synchronous cancer imaging and traceable drug delivery, as well as cRGD ligands were coupled onto micelle surface for targeting integrin $\alpha_v\beta_3$ of tumor endothelial cells (79). The integrated micelle conjugates showed increased uptake *in vitro* $\alpha_v\beta_3$-overexpressing endothelial cells. In a further study, they provided noninvasive imaging of tumor angiogenesis in human lung cancer subcutaneous tumor xenografts with $\alpha_v\beta_3$-specific nanoprobe consisting of fluorescent superparamagnetic polymeric micelles (FSPPM) (80). MRI data showed $\alpha_v\beta_3$-specific FSPPM accumulation at tumor site *in vivo*, allowing for an accurate and quantitative characterization of tumor angiogenesis.

The great advantage of polymeric micelles is that they can encapsulate relatively higher amount of hydrophobic drugs and imaging agents but remain its high water solubility as a carrier comparing to other alternatives such as soluble polymers and liposomes. Along with the successful application in therapeutics in preclinical and clinical studies, polymeric micelles are also accepted as multifunctional delivery systems that may maximize the therapeutic efficacy and reach goals in personalized medicine.

Liposomes

Liposomes are the most clinically established nanoplatform systems for incorporation of targeting, imaging, drug and gene delivery entities (81). Various liposomes are approved by the FDA to carry a range of chemotherapeutics for different therapeutic indications. Two well known formulations are Caelyx/Doxil and Myocet, which are PEGylated liposomal doxorubicin products that attenuate drug-related toxicity, but keep the formulation having similar therapeutic effects as free ones. This is exemplified by the results from clinical trials, in which it was demonstrated that cardiotoxicity can be significantly reduced, but its response rates and time to progression were substantially comparable to conventional doxorubicin in treatment of metastatic breast carcinoma (82,83). One significant obstacle of liposome systems is that the encapsulated drug within a liposome is difficultly released at the intended site. To address this problem, new generations of liposome systems have been developed to trigger drug release from liposome cavities at specific sites by change in pH, temperature or certain actions of enzymes on liposome surface (84,85). ThermoDox, a liposomal formulation, encapsulated doxorubicin within a temperature-sensitive liposome, is currently in a Phase II clinical trial for combination use with hyperthermia treatment in oncology (86).

A wide range of therapeutics can be encapsulated in their aqueous volume or embedded within the bilayer of liposomes. One straightforward approach for incorporation of contrast agents into liposomes is relying on a chelating ligand labeled with either a MRI contrast agent Gd^{3+}, or a selected radionuclide for PET or SPECT nuclear imaging (87). In a few reports, novel tumor targeting liposomal complexes incorporated contrast agents result in multifunctional theranostic nanoplatforms for the combined detection of early diseases and monitoring of drug delivery (88–90). For example, Kenny *et al.* showed therapeutic siRNA-entrapped liposomes combining MR with fluorescence microscopy imaging for real-time monitoring of drug delivery and therapeutic effects *in vivo* (88). In addition, magnetic nanoparticle can be encapsulated inside liposomes as theranostic nanosystems (91). Plank research group designed folate receptor targeted thermosensitive magnetic liposomes entrapped doxorubicin for hyperthermia treatment of cancer in conjunction with chemotherapy (92). The multifunctional liposome showed that magnetic hyperthermia can trigger doxorubicin release from liposomes with improved tumor cell killing in comparison to non-magnetic folate-targeted liposomes and Caelyx®.

From many examples, multifunctional theranostic liposomes have been used for detection or treatment of diseases, and they will be chosen as promising carriers for further enhancement of therapeutic and diagnostic efficacy.

Dendrimers

Dendrimers are unqiue macromolecules with precise controlled structures. Their size can be finely tuned by adjusting the number of generations, and therapeutics or imaging moieties can be added with good loading efficiency through optimal design of conjugation sites. These unique features

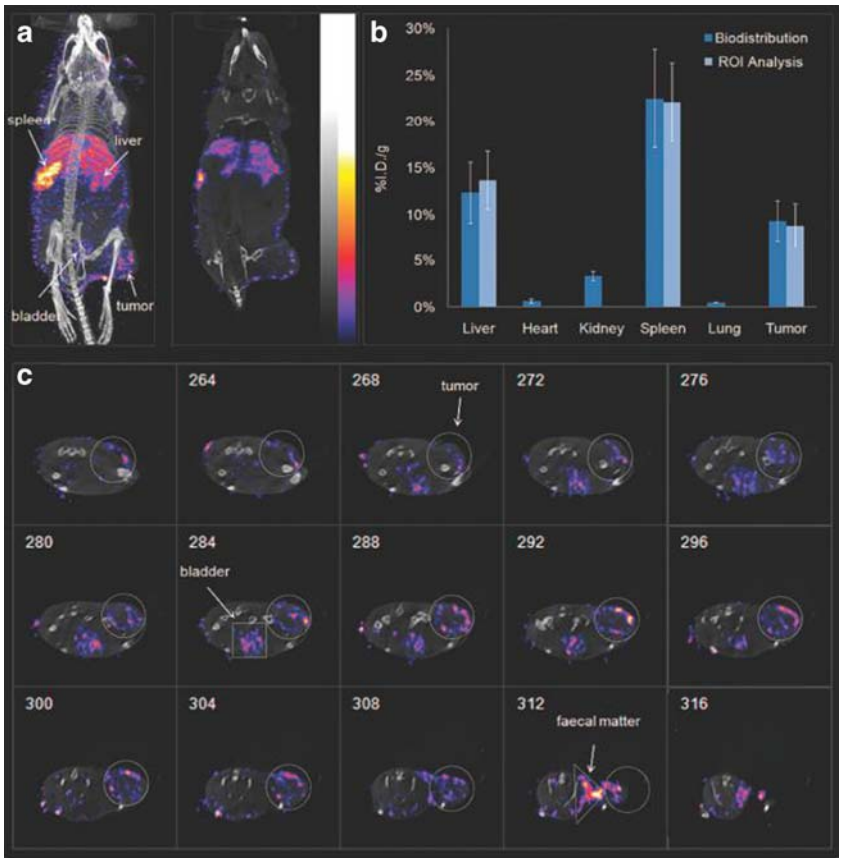

Fig. 4 (**a**) MicroSPECT/CT imaging of athymic mice bearing MDA-MB-231 breast cancer xenografts after 48 h iv administration of ^{111}In-micelles. The accumulation of ^{111}In-micelles in the liver, spleen, bladder and tumor was clearly visualized on the images. (**b**) The ^{111}In-micelles quantification of tissue accumulation via γ-counting and MicroSPECT/CT region-of-interest (ROI) analyses in MDA-MB-231 tumor-bearing mice at 48 h p.i. (**c**) The tumor radioactivity on the transverse slices displayed the nonhomogeneous distribution of ^{111}In-micelles. Images adapted with permission from refs (72)

have made dendrimers of increasingly important as theranostic nanoplatforms. Dendrimers are capable of non-covalently or covalently binding of chemotherapy drugs, imaging agents, and other biologically active targeting moieties such as monoclonal antibodies, peptides and folate (93–95). Thomas *et al*. have demonstrated that a generation 5 polyamidoamine (PAMAM) dendrimer conjugated with both folic acid (FA) and methotrexate (MTX) has better chemotherapeutic efficiency than MTX alone (96). In our previous report, a series of Gd(III)-based peptide dendrimers with highly controlled structures can be used as efficient multivalent MRI probes (97,98). *In vivo* studies have shown that the mPEGylated Gd(III)-based dendrimer provided much longer blood circulation time and higher signal intensity enhancement in mouse kidney comparing to other dendrimer formulations.

The unique structural properties allow dendrimers can be used to stabilize hydrophobic nanoparticles through the ligand-exchange reaction method. This strategy had been applied to directly exchange the original organic ligands from SPIO nanoparticles with hydrophilic ligands based on various functional groups as the anchoring groups (99–101). Chang *et al*. has developed a novel multifunctional PAMAM dendrimer-based carrier conjugated to SPIO nanoparticles for imaging and doxorubicin through a pH-sensitive hydrazone linker for therapy, which showed good biocompatibility, biodistribution, and satisfactory cancer imaging results (102). And the stimuli-responsive dendrimers have shown better control of drug release at the disease site, but remain relatively stable in the systemic circulation. In another example, dendrimers are used to entrap Au nanoparticles or modify the surface of Au nanoparticles for CT imaging application (103). Multimodality dendrimers can be achieved by designed surface modification to form MR, CT or PET/SPECT imaging agents (104).

Dendrimers can be chosen as carriers of chemotherapy drugs or imaging agent through conjugation, and they can also be used to form complex with therapeutic DNA/RNA (105,106). In one example, Yu synthesised PAMAM dendron modified with hydrophobic alkyl chains for effective delivery of Hsp27 siRNA *in vitro* and *in vivo* in a castration-resistant prostate cancer model, and produce significant gene silencing and potent anticancer activity (107).

Although dendrimers have proven to be successful drug and imaging agent carriers in a number of preclinical studies, however, dendrimers are more expensive than other nanoparticles and require many repetitive steps for synthesis, posing a challenge for large-scale production. While cationic

polymer/DNA complexes showed unexpected characteristics such as short plasma circulation times, low transfection efficiencies *in vivo* compared to viral vector, and inherent cytotoxicity associated with their cationic nature (108).

APPLICATIONS IN CANCER

According to World Health Organization in 2008, cancer affects tens of millions people in all age groups and both sexes as a disease (109). Although diagnostic procedures and conventional treatment technologies have made significant strides in clinical applications, they remain far from optimal. Over the past decade, there has been a burst of interest in development of nanoparticle-based theranostics for imaging of early-stage cancer and drug delivery simultaneously. A number of excellent review articles are available on nanoparticle-based theranostic systems (110–112). Here, we will briefly introduce some examples to illustrate the feasibility of simultaneous imaging drug distribution and controlling drug release at a target site, as well as monitoring of therapeutic efficacy.

Imaging of Pharmacokinetics and Targeted Drug Delivery

The properties of pharmacokinetics and biodistribution of drugs determine the efficacy of chemotherapy and radiotherapy, as well as the safety of the treatment. Theranostics based on nanoparticles play an increasingly important role in non-invasive monitoring of key properties of various diseases, including cancers. And high sensitivity PET or SPECT imaging is a valuable technique that can provide noninvasive longitudinal visualization of pharmacokinetics and tissue deposition. For example, Cai, Gong and colleagues recently designed a multifunctional micelle (H40-DOX-cRGD-^{64}Cu) made of a hyperbranched amphiphilic block copolymer conjugated with targeting ligands and imaging agents for cancer-targeted drug delivery and non-invasive PET imaging in tumor-bearing mice, while DOX was covalently conjugated onto polymer via an acid-labile hydrazone linkage to control drug release (113). In this report, researchers studied the drug release *in vitro* under simulated physiological and cellular conditions confirming that the amount of DOX released from the H40-DOX-cRGD-^{64}Cu at pH values of 5.3 and 6.6 far exceed that at pH values of 7.4 after 45 h (92.7%, 85.6 and 12.1% respectively). Further flow cytometry and confocal laser scanning microscopy analysis revealed that H40-DOX-cRGD-^{64}Cu substantially increased the cellular uptake exhibiting a 90% higher level than cells treated with H40-DOX-^{64}Cu after 2 h incubation. For *in vivo* experiment, PET imaging (Fig. 5) displayed that the nanocomposites primarily accumulated in the liver, tumor, lung, kidney and intestines in three experimental groups, but H40-DOX-cRGD had higher U87MG tumor-targeting efficacy and provided faster and better visualization comparing to H40-DOX-cRGD with a blocking dose of cRGD peptide and H40-DOX respectively after intravenous injection. Quantitative data obtained from ROI analyses further confirmed that the U87MG tumor uptake of H40-DOX-cRGD was tend to be twice as high as H40-DOX-^{64}Cu.

Imaging of Drug Release

It's worth highlighting that it is important to visualize and analyze drug release under simulated *in vitro* conditions, however, a direct evaluation under physiologically relevant *in vivo* conditions is a far more important clinical demand in drug delivery. Several research groups have been working on strategies for noninvasive visualization or quantification of drug release *in vivo* over the past few years, and almost all of analytical methods are indirectly by MRI with gadolinium-based contrast agents (114–117). MRI can be used to detect varied signal intensities caused by the changing interaction between surrounding water molecules and gadolinium-based contrast agents within *versus* outside of water-impermeable nanoparticles, thus to monitor drug release using gadolinium chelate as a surrogate diffusible tracer (118). Nonetheless, the studied drug should be similar to a gadolinium agent with regard to factors such as molecular size, hydrophilicity, and other physicochemical characteristics (119).

Li and colleagues developed a thermosensitive liposome (HaT) co-encapsulating Gd-DTPA and DOX which enables simultaneous real-time monitoring of drug delivery and release in a locally heated tumor (120). Figure 6a illustrates that when the formulation was incubated under 37°C in 30 min, no T_1 imaging reduction was observed, while heated at 40 and 42°C for 1–3 min, T_1 signal reduced 60% equivalent to the Triton X-100 treated samples, and representing full release of Gd-DTPA. From the release kinetics of Gd-DTPA and DOX measured by MRI and fluorescence respectively (Fig. 6b, c), we can see DOX was completely released at 40–42°C within 3 min, but negligible drug leakage at 30–37°C over 30 min. These results indicated that DOX release profile from liposome *in vitro* was closely related to the release of Gd-DTPA, corresponding to the change in the MR T_1 relaxation time. Based on the above reasoning, they quantify the release of DOX before and after heating treatment by the change of MR T_1 signal in mammary carcinoma tumor-bearing mice. Figure 6d shows that T_1-weighted MR signal intensity in the heated tumor was significantly decreased after treatment, but few changes in the contralateral unheated tumor.

Imaging of Therapeutic Efficacy

Besides for visualizing drug delivery and release at primary and metastatic cancer, nanoparticle-based theranostic

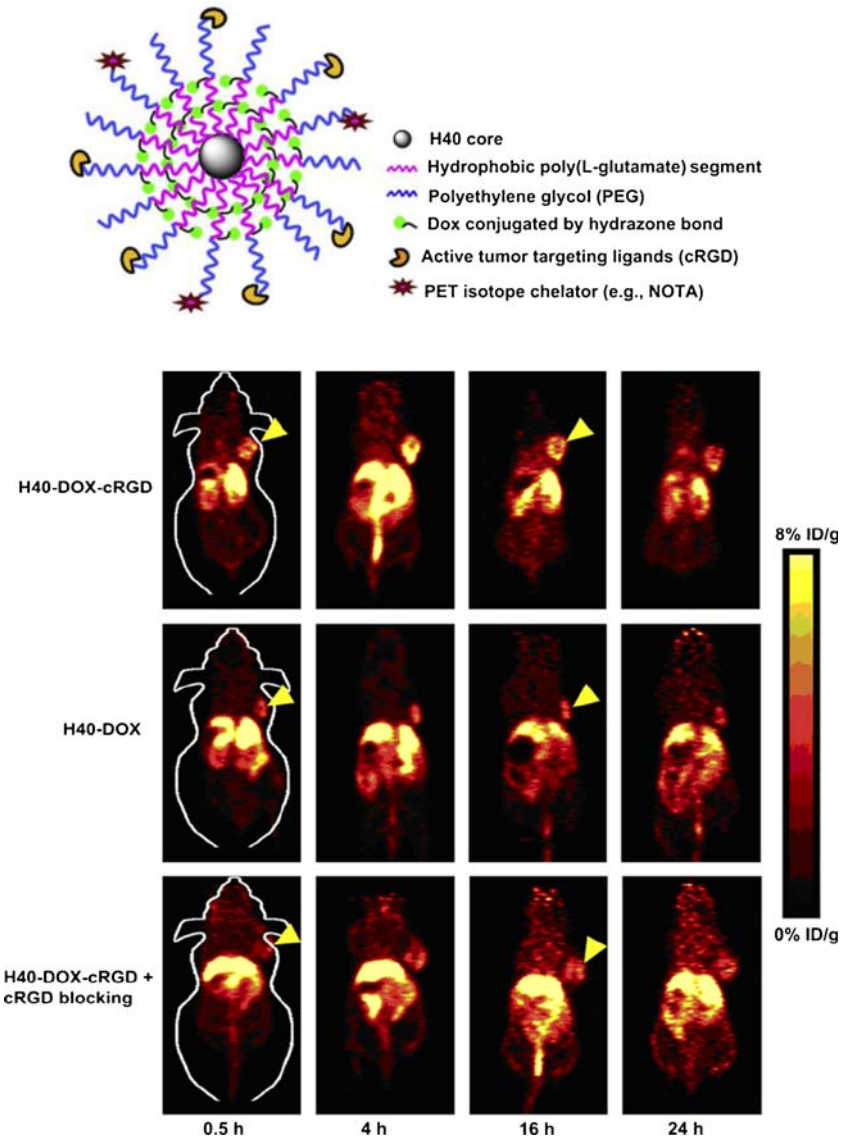

Fig. 5 *Top* A schematic illustration of the multifunctional H40-DOX-cRGD-^{64}Cu nanocomposites for tumor-targeted drug delivery and PET imaging. *Bottom* PET imaging of U87MG tumor-bearing mice at various time points post-injection of H40-DOX-^{64}Cu, H40-DOX-cRGD-^{64}Cu, or H40-DOX-cRGD-^{64}Cu with a blocking dose of cRGD. Images adapted with permission from refs (113).

applications have been expanded for imaging of tumor progression and therapy response. Changes in tumor dimension, angiogenesis, antigen expression, and expression of specific molecular markers etc., are important indicators for therapeutic efficacy analysis (121,122).

Nanoparticle-based theranostics offer tangible options to better evaluate the drug effect and track tumor size over time using PET or MRI imaging modalities. For example, Kaida group designed a multifunctional polymeric micellar nanocarrier incorporating Gd-based contrast agents and platinum (Pt) anticancer drugs through reversible metal chelation of Pt (Gd-DTPA/DACHPt-loaded micelles), simultaneous for imaging and therapy of an orthotopic animal model of intractable human pancreatic tumor (123). In the research, they assessed the antitumor activity of Gd-DTPA/DACHPt-loaded micelles by monitoring the tumor size in real-time using T1W T_1-weighted MR imaging at the day of the drug administration. MR images indicated that the tumor size of the mice have a significant reduction after 18 days treated with the micelles at 8 mg/kg on Pt base. In another example, William et.al used contrast-enhanced MRI scan to reflect visually the tumor size, and then evaluated the brachytherapy activity of rhenium-186 (^{186}Re)-liposomes by convection-enhanced delivery in an orthotopic U87 glioma rat model (Fig. 7) (124). The images depicted the significant efficacy of ^{186}Re-liposomal brachytherapy that the tumor size decrease or even disappear with increased therapeutic duration, whereas, the marked difference in tumor size was observed between the groups that without treatment for 14 days.

Clinical and experimental studies suggest that angiogenesis is a prerequisite in the process of solid tumor growth and metastatic dissemination (125–127). Tumor angiogenesis could be utilized for treatment of tumor through antiangiogenic therapy and for assessment of tumor

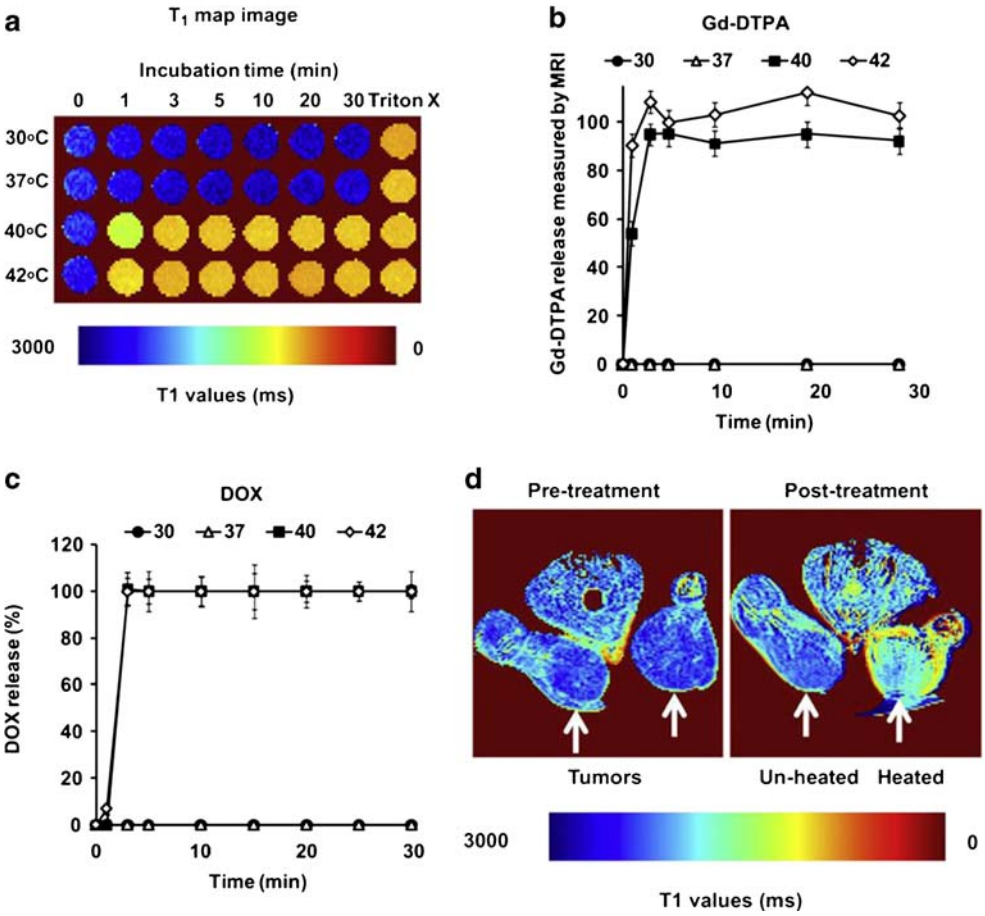

Fig. 6 (**a**) T_1 image of HaT *in vitro* after incubation at different temperatures. Triton X-100 was used to completely release Gd-DTPA and DOX. Rainbow bar = T_1 value (ms). (**b**) The release kinetics of Gd-DTPA from HaT after incubation at different temperatures. (**c**) The release kinetics of DOX from HaT after incubation at different temperatures. Data are mean ± S.D ($n = 3$). (**d**) T_1 images of the tumor xenografts before and after treated with HaT (10 mg DOX/kg) in combination with local hyperthermia to one tumor. Images adapted with permission from refs (120).

progression by non-invasive imaging (128,129). The $\alpha_v\beta_3$ integrin receptor plays an important role in pathologic angiogenesis associated with tumor progression and metastasis. Targeting this receptor may assess integrin expression level and improve drug delivery efficiency.

Chen and Lu developed a MRI probe by decoration of RGD peptides on iron oxide nanoparticles with a crosslinked PEGylated amphiphilic triblock polymer (IONP-RGD), for noninvasive monitoring of the antiangiogenic therapy response of a vascular disrupting agent $VEGF_{121}$/rGel in an

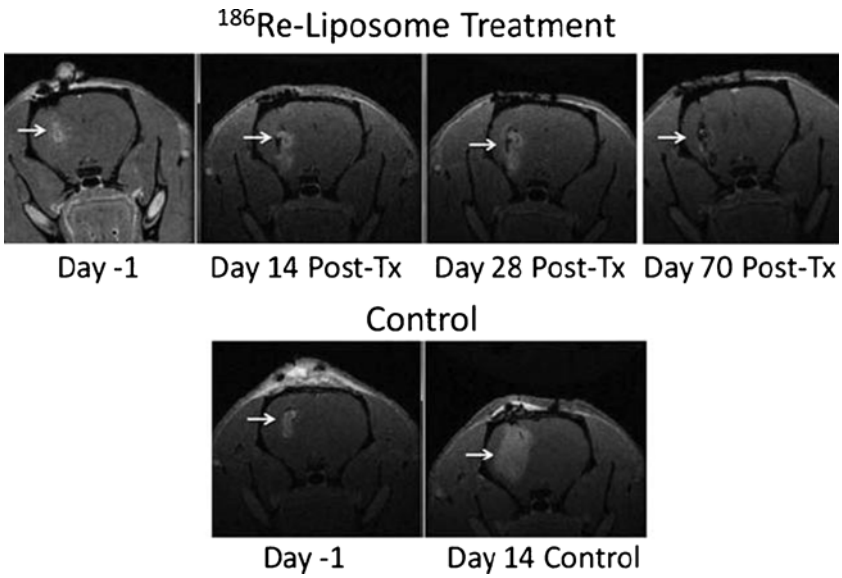

Fig. 7 *In vivo* antitumor activity of ^{186}Re-liposomal on orthotopic U87 glioma model assessed by contrast-enhanced MRI. Images adapted with permission from refs (124)

orthotopic U87MG glioblastoma model (130). For treatment evaluation, two doses of 12 mg/kg VEGF121/rGel were intraperitoneally administered. After 4 days treatment, the signal of IONP-RGD after 6 h post-injection in tumor areas was obviously decreased in the treated group comparing to pre-injection signals (Fig. 8a). Dynamic T_2*-weighted imaging at various time points from 0 to 70 min were displayed in Fig. 8b. A fast and obvious signal enhancement of IONP-RGD was observed in tumor areas of the untreated group, but a small signal intensity decrease was detected in the treated group. These results demonstrated the $VEGF_{121}$/rGel damaged tumor angiogenic blood vessels and inhibited integrin expression. More importantly, using IONP-RGD for noninvasive imaging has higher sensitivity than traditional approaches based on measurement of tumor size, monitoring of early tumor responses to antiangiogenic therapies.

Not limited for loading of small molecule anticancer drugs, imaging visible nanoparticles have also demonstrated their capability of carrying biomacromolecules such as therapeutic genes. For example, polycation/SPIO nanocomposites were used as MRI visible carriers for delivery of siRNA both *in vitro* and *in vivo* (131). In that study, multiple hydrophobic SPIO nanocrystals are self-assembled into cationic nanocomposites (alkyl-PEI2k-IO) in water phase with a low molecular weight alkylated polyethyleneimine (alkyl-PEI2k). Alkyl-PEI2k-IOs can form complexes with luciferase siRNA and induce enhanced down regulation of luciferase in fluc-4 T1 cells without exhibiting cellular toxicity *in vitro*. Meanwhile, at a 7 T magnetic field, the transfected cells displayed strong signal contrast compared to untreated cells on T_2 weighted imaging. During *in vivo* studies, the alkyl-PEI2k-IOs/siRNA complexes demonstrated remarkable gene silencing efficiency on a 4 T1-fluc tumor xenograft model.

APPLICATION IN CARDIOVASCULAR DISEASE

Cardiovascular disease (CVD) encompasses a class of diseases, many of which are related to a process called atherosclerosis and its sequelae, including myocardial infarction and cerebrovascular accidents. CVD is the leading cause of mortality, representing a substantial economic burden (132). The practice of clinical imaging technology makes remarkable advances for diagnosis of CVD, but problems need to be solved including how to accurately distinguish the vulnerability and the rupture of atherosclerotic plaques, as well as monitor the effect of innovative therapies of heart failure (133,134). The availability of multifunctional nanoplatform-based theranostics represents a potential solution for these problems (135,136).

Given that the considerable mortality is primarily due to plaque destabilization, early detection is crucial for preventing of myocardial infarction and sudden cardiac death. The initiation of plaque rupture has been linked to fibrin deposition, plaque neovasculature, as well as abundance of macrophages that contribute to the degradation of the fibrous cap by upregulation of metalloproteinases (137). These characteristics offer a few potential targets allowing for the construction of functional diagnostic or therapeutic agents, including nanoplatform-based theranostic agents.

Atherosclerotic plaque development and progression of the disease is accompanied by neovascularization of the vessel wall (138). Angiogenesis is associated with plaque hemorrhage, and intraplaque hemorrhage play a role in atherosclerotic plaque growth and destabilization (139–141). Therefore, angiogenesis is a potential therapeutic target for plaque stabilization. Lanza *et al.* studied the potential of paramagnetic nanoparticles that incorporated fumagillin for noninvasive assessment of $\alpha_v\beta_3$-integrin expression and quantification of local response to treatment in a rabbit model of atherosclerosis (142). This study showed that the $\alpha_v\beta_3$-targeted paramagnetic nanoparticles with and without fumagillin displayed more increased MR signal intensity in the aortic wall compared to the nontargeted nanoparticles (16.7%, 16.7%, and 10.8% respectively) after 4 h post-administration of the nanoparticles. One week following the antiangiogenic nanoparticle treatment, $\alpha_v\beta_3$-targeted paramagnetic nanoparticles were readministered and T_1-weighted MR signal enhancement in the aortic wall revealed a significant decrease (2.9%), but not in untreated rabbits (18.1%). Collectively, these data suggest that $\alpha_v\beta_3$-targeted paramagnetic nanoparticles delivery of fumagillin might inhibit the regeneration process of neovasculature within the aortic wall, and the therapeutic efficacy can be noninvasively assessed by MRI.

Plaques contain numerous inflammatory cells, in particular macrophages that can lead to inflammatory atherosclerotic plaques destabilization and disruption, resulting in myocardial infarction and stroke (143). Targeting of macrophages is an appealing approach to analyze and treat vulnerable plaques prone to clinical complications (144). Mulder group developed a multimodal imaging nanomedicinal liposomal formulation of glucocorticoids (L-PLP) to deliver the drug into atherosclerotic plaques, as well as to monitor delivery and rapid anti-inflammatory effects in atherosclerotic lesions (Fig. 9a) (145). Figure 9b showed a marked T_1-weighted MRI signal intensity increase throughout the entire inflamed vessel wall 2 days after the administration, indication of a considerable accumulation of liposomes at the atherosclerotic lesions. ^{18}F-FDG-PET/CT was used to track therapeutic effects of L-PLP in atherosclerotic rabbits by visualizing and quantifying plaque macrophage inflammation. Figure 9c revealed a clearly visible signal enhancement throughout the aorta before treatment with L-PLP, but a significant reduction of ^{18}F-FDG uptake after 1 week of treatment, demonstrating the efficacy of L-PLP. Dynamic contrast enhanced MRI (DCE-MRI) also proved the efficacy of L-PLP (Fig. 9d). The

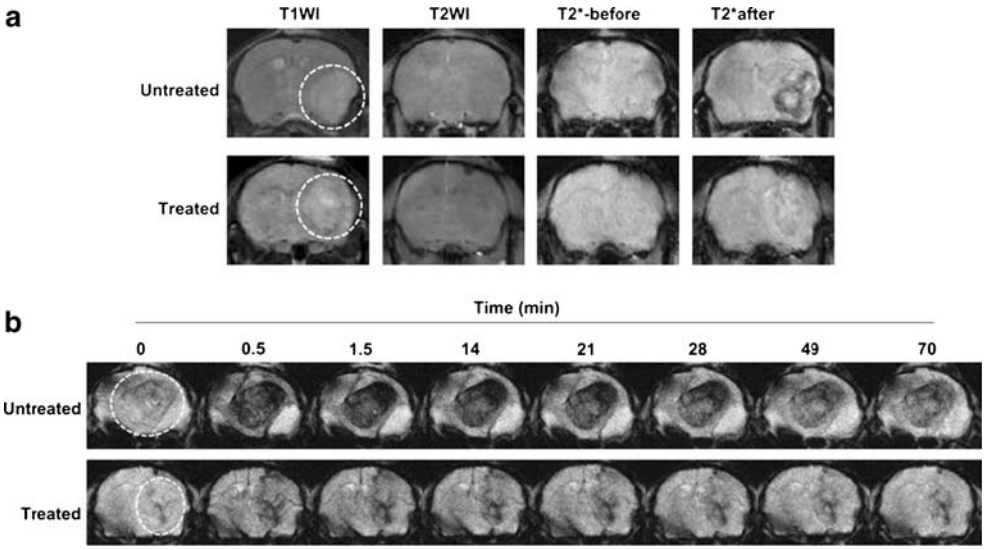

Fig. 8 Monitoring of therapeutic response of $VEGF_{121}$/rGel in orthotopic U87MG glioblastoma model by MRI. (**a**) T_2*-weighted MR imaging of untreated and $VEGF_{121}$/rGel treated groups before and after 6 h post-injection of IONP-RGD. (**b**) T_2*-weighted MR dynamic imaging of untreated and $VEGF_{121}$/rGel treated groups before and after injection of IONP-RGD. The *white circle* indicates location of the implanted tumor (4 mice each group). Images adapted with permission from refs (130)

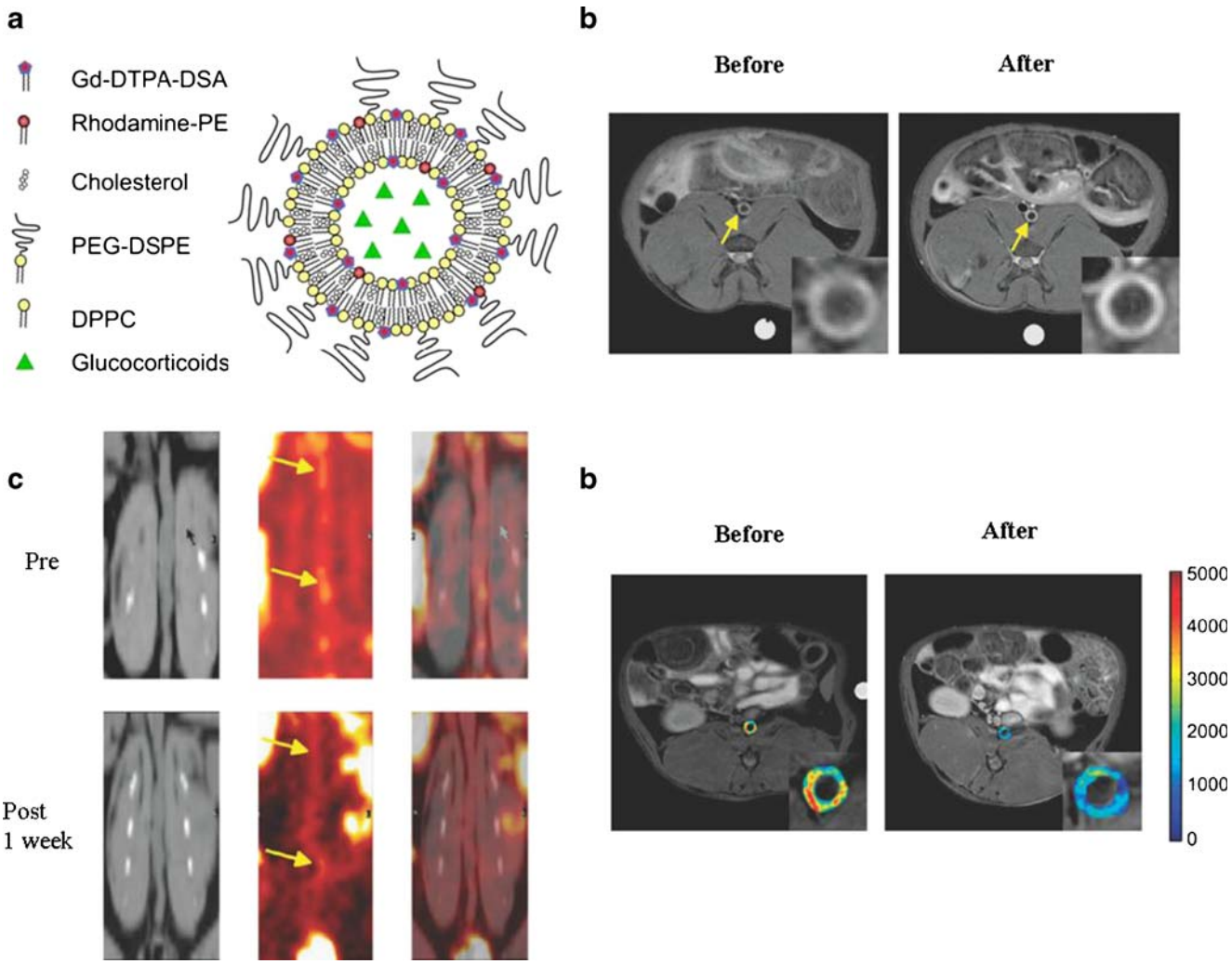

Fig. 9 (**a**) Schematic of the liposomal nanoparticle (L-PLP). (**b**) MR images of the abdominal aortic wall before and 2 days after the administration of L-PLP in atherosclerotic rabbits. (**c**) PET/CT images of the abdominal aortic wall before and 1 week after the administration of liposomal PLP for evaluating therapeutic effects. (**d**) DCE-MR overlays images of the abdominal aortic wall before treatment and 2 days post-treatment with L-PLP. Images adapted with permission from refs (145)

area under the curve (AUC) of the vessel wall showed a more obvious decrease 2 days post-injection of L-PLP (1784±449 AU) comparing to pre-injection (2278±406 AU).

Coronary stents have greatly reduced the risk of restenosis since their clinical introduction. Nevertheless, restenosis still occurs in a substantial proportion of patients and how to develop effective theranostic agents remain a great challenge in pharmaceutical industry (146). It is possible that nanoparticle-based theranostics can provide a novel approach to improve clinical outcome (147,148). PFC nanoparticles, previously considered as artificial blood substitutes (149), have been developed into a nanoplatform technology for targeting drug delivery and quantitative detection with the help of MR imaging and spectroscopy of its fluorine (^{19}F) core (150). Lanza group designed $\alpha_v\beta_3$-targeted PFC nanoparticles with rapamycin for inhibiting restenosis after balloon injury, and imaging therapeutic effects (151). The study indicated that the segments at 2 weeks after treatment with $\alpha_v\beta_3$-targeted rapamycin nanoparticles had a widely patent contralateral artery, while the control segments had sensible lumen irregularities. Histological analysis also revealed reduced restenosis in all injured arteries segments that treated with targeted drug nanoparticles. These data confirmed $\alpha_v\beta_3$-targeted rapamycin nanoparticle can be locally delivered into the stretch-fractured arteries, and thus reduce stenosis response.

CONCLUSION AND PERSPECTIVE

The field of theranostics remains relatively young, but considerable efforts have been made toward the research and development of theranostic nanoparticles for cancer and cardiovascular targeted imaging and therapy. Of various theranostic nanoplatforms, biodegradable and metabolizable polymer nanoparticles have been designed and tested in small animal models. Advantages of these particles include long circulation life, good biosafety, decoration of targeting moieties, and loading of therapeutic and contrast agents. These multifunctional polymer nanoparticles can be used for noninvasive diagnosis of certain diseases with anatomical details. Besides, one can assess the pharmacokinetics, biodistribution and targeting efficiency of conjugated or entrapped therapeutic agents, and therapeutic responses. These functions can facilitate the development of novel drugs in both preclinical and clinical phases.

Nevertheless, the translation of such a system to clinical success faces many barriers, especially the low drug loading capacity and drug concentrations in the lesion locations. Currently, the drug loading in most nanoparticles is usually around 10%, and usually less than 2% of the total administered nanoparticles arrives at the tumor site even if the periphery of polymer nanoparticles conjugated with targeting ligands (152). In this respect, the amount of the drug accumulated to the target lesion locations may be the same for both targeting and non-targeting formulations. But one may find solutions for improved drug targeting efficiency by other mechanisms down the road. Moreover, the costs and regulatory hurdles associated with adding targeting ligands and imaging capabilities to nanoparticles are additional consideration for commercial viability. However, it is important that nanoparticle approach can reduce drug toxicity and provide an alternative way for intravenous administration of poorly soluble drugs, and it may offset the costs. In addition, the clinical demand for simultaneous imaging and therapeutic capabilities will likely drive the further investment on theranostic agents. Theranostic nanoparticles may be used in clinic in the near future for providing extra values on diagnosis and therapeutic efficacy evaluation of cancer and cardiovascular patients.

ACKNOWLEDGMENTS AND DISCLOSURES

The work was supported by National Key Basic Research Program of China (2013CB933903), National Key Technology R&D Program (2012BAI23B08), Doctoral Fund of Ministry of Education of China (20090181110068) and National Natural Science Foundation of China (20974065, 51173117 and 50830107).

REFERENCES

1. Sun D. Nanotheranostics: integration of imaging and targeted drug delivery. Mol Pharm. 2010;7(6):1879.
2. Kievit FM, Zhang M. Cancer nanotheranostics: improving imaging and therapy by targeted delivery across biological barriers. Adv Mater. 2011;23(36):H217–47.
3. Kelkar SS, Reineke TM. Theranostics: combining imaging and therapy. Bioconjugate Chem. 2011;22(10):1879–903.
4. Ahmed N, Fessi H, Elaissari A. Theranostic applications of nanoparticles in cancer. Drug Discov Today. 2012;17(17–18):928–34.
5. Davis ME, Chen Z, Shin DM. Nanoparticle therapeutics: an emerging treatment modality for cancer. Nat Rev Drug Discov. 2008;7(9):771–82.
6. Mi Kyung Yu JP, Jon S. Targeting strategies for multifunctional nanoparticles in cancer imaging and therapy. Theranostics. 2012;2(1):3–44.
7. Lammers T, Kiessling F, Hennink WE, Storm G. Nanotheranostics and image-guided drug delivery: current concepts and future directions. Mol Pharm. 2010;7(6):1899–912.
8. Peer D, Karp JM, Hong S, FaroKhzad OC, Margalit R, Langer R. Nanocarriers as an emerging platform for cancer therapy. Nat Nanotechnol. 2007;2(12):751–60.
9. Duncan R. The dawning era of polymer therapeutics. Nat Rev Drug Discov. 2003;2(5):347–60.
10. Tong R, Cheng JJ. Anticancer polymeric nanomedicines. Polym Rev. 2007;47(3):345–81.
11. Bae KH, Chung HJ, Park TG. Nanomaterials for cancer therapy and imaging. Mol Cell. 2011;31(4):295–302.

12. Sahoo SK, Labhasetwar V. Nanotech approaches to delivery and imaging drug. Drug Discov Today. 2003;8(24):1112–20.
13. Pysz MA, Gambhir SS, Willmann JK. Molecular imaging: current status and emerging strategies. Clin Radiol. 2010;65(7):500–16.
14. Ai H. Layer-by-layer capsules for magnetic resonance imaging and drug delivery. Adv Drug Deliver Rev. 2011;63(9):772–88.
15. Cai WB, Rao JH, Gambhir SS, Chen XY. How molecular imaging is speeding up antiangiogenic drug development. Mol Cancer Ther. 2006;5(11):2624–33.
16. Jokerst JV, Gambhir SS. Molecular imaging with theranostic nanoparticles. Accounts Chem Res. 2011;44(10):1050–60.
17. Janib SM, Moses AS, MacKay JA. Imaging and drug delivery using theranostic nanoparticles. Adv Drug Deliver Rev. 2010;62(11): 1052–63.
18. Willmann JK, van Bruggen N, Dinkelborg LM, Gambhir SS. Molecular imaging in drug development. Nat Rev Drug Discov. 2008;7(7):591–607.
19. Rudin M, Weissleder R. Molecular imaging in drug discovery and development. Nat Rev Drug Discov. 2003;2(2):123–31.
20. Wong DF, Tauscher J, Grunder G. The role of imaging in proof of concept for CNS drug discovery and development. Neuropsychopharmacology. 2009;34(1):187–203.
21. Cai W, Wu Y, Chen K, Cao Q, Tice DA, Chen X. In vitro and in vivo characterization of ^{64}Cu-labeled Abegrin™ a humanized monoclonal antibody against integrin $\alpha_v\beta_3$. Cancer Res. 2006;66(19):9673–81.
22. Niu G, Sun X, Cao Q, Courter D, Koong A, Le QT, *et al.* Cetuximab-based immunotherapy and radioimmunotherapy of head and neck squamous cell carcinoma. Clin Cancer Res. 2010;16(7):2095–105.
23. Weiler Sagie M, Bushelev O, Epelbaum R, Dann EJ, Haim N, Avivi I, *et al.* ^{18}F-FDG avidity in lymphoma readdressed: a study of 766 patients. J Nucl Med. 2010;51(1):25–30.
24. Lardinois D, Weder W, Hany TF, Kamel EM, Korom S, Seifert B, *et al.* Staging of non-small-cell lung cancer with integrated positron-emission tomography and computed tomography. New Engl J Med. 2003;348(25):2500–7.
25. Pelosi E, Deandreis D. The role of 18F-fluoro-deoxy-glucose positron emission tomography (FDG-PET) in the management of patients with colorectal cancer. Eur J Surg Oncol. 2007;33(1):1–6.
26. J Nucl Med op. FDA approves 18F-florbetapir PET agent. J Nucl Med. 2012; 53(6): 15N–15N.
27. Cain SM, Ruest T, Pimlott S, Patterson J, Duncan R, Dewar D, *et al.* High resolution micro-SPECT scanning in rats using ^{125}I β-CIT: Effects of chronic treatment with carbamazepine. Epilepsia. 2009;50(8):1962–70.
28. Zhou J, Yu MX, Sun Y, Zhang XZ, Zhu XJ, Wu ZH, *et al.* Fluorine-18-labeled $Gd^{3+}/Yb^{3+}/Er^{3+}$ co-doped $NaYF_4$ nanophosphors for multimodality PET/MR/UCL imaging. Biomaterials. 2011;32(4): 1148–56.
29. Pichler BJ, Kolb A, Nagele T, Schlemmer HP. PET/MRI: paving the way for the next generation of clinical multimodality imaging applications. J Nucl Med. 2010;51(3):333–6.
30. Pichler BJ, Wehrl HF, Kolb A, Judenhofer MS. Positron emission tomography/magnetic resonance imaging: the next generation of multimodality imaging? Semin Nucl Med. 2008;38(3):199–208.
31. Antoch G, Bockisch A. Combined PET/MRI: a new dimension in whole-body oncology imaging? Eur J Nucl Med Mol Imaging. 2009;36 Suppl 1:S113–20.
32. Wehrl HF, Judenhofer MS, Wiehr S, Pichler BJ. Pre-clinical PET/MR: technological advances and new perspectives in biomedical research. Eur J Nucl Med Mol Imaging. 2009;36 Suppl 1:S56–68.
33. Zweifel M, Padhani AR. Perfusion MRI in the early clinical development of antivascular drugs: decorations or decision making tools? Eur J Nucl Med Mol Imaging. 2010;37 Suppl 1:S164–82.
34. Murphy SE, Mackay CE. Using MRI to measure drug action: caveats and new directions. J Psychopharmacol. 2011;25(9):1168–74.
35. Kalber TL, Kamaly N, Higham SA, Pugh JA, Bunch J, McLeod CW, *et al.* Synthesis and characterization of a theranostic vascular disrupting agent for in vivo MR imaging. Bioconjug Chem. 2011;22(5):879–86.
36. Gupta AK, Gupta M. Synthesis and surface engineering of iron oxide nanoparticles for biomedical applications. Biomaterials. 2005;26(18):3995–4021.
37. Xie J, Liu G, Eden HS, Ai H, Chen X. Surface-engineered magnetic nanoparticle platforms for cancer imaging and therapy. Acc Chem Res. 2011;44(10):883–92.
38. Wolf W, Albright MJ, Silver MS, Weber H, Reichardt U, Sauer R. Fluorine-19 NMR spectroscopic studies of the metabolism of 5-fluorouracil in the liver of patients undergoing chemotherapy. Magn Reson Imaging. 1987;5(3):165–9.
39. Wolf W, Waluch V, Presant CA. Non-invasive ^{19}F-NMRS of 5-fluorouracil in pharmacokinetics and pharmacodynamic studies. NMR Biomed. 1998;11(7):380–7.
40. Chen J, Lanza GM, Wickline SA. Quantitative magnetic resonance fluorine imaging: today and tomorrow. WIREs Nanomed Nanobi. 2010;2(4):431–40.
41. Noth U, Morrissey SP, Deichmann R, Jung S, Adolf H, Haase A, *et al.* Perfluoro-15-crown-5-ether labelled macrophages in adoptive transfer experimental allergic encephalomyelitis. Artif Cell Blood Sub. 1997;25(3):243–54.
42. Srinivas M, Turner MS, Janjic JM, Morel PA, Laidlaw DH, Ahrens ET. *In vivo* cytometry of antigen-specific t cells using ^{19}F MRI. Magn Reson Med. 2009;62(3):747–53.
43. Ruiz-Cabello J, Barnett BP, Bottomley PA, Bulte JW. Fluorine (^{19}F) MRS and MRI in biomedicine. NMR Biomed. 2011;24(2):114–29.
44. Greco F, Vicent MJ. Combination therapy: opportunities and challenges for polymer-drug conjugates as anticancer nanomedicines. Adv Drug Deliver Rev. 2009;61(13):1203–13.
45. Canal F, Sanchis J, Vicent MJ. Polymer-drug conjugates as nano-sized medicines. Curr Opin Biotech. 2011;22(6):894–900.
46. Manchun S, Dass CR, Sriamornsak P. Targeted therapy for cancer using pH-responsive nanocarrier systems. Life Sci. 2012;90(11–12): 381–7.
47. Hoffman AS, Stayton PS. Conjugates of stimuli-responsive polymers and proteins. Prog Polym Sci. 2007;32(8–9):922–32.
48. Duncan R. Polymer conjugates as anticancer nanomedicines. Nat Rev Cancer. 2006;6(9):688–701.
49. Larson N, Ghandehari H. Polymeric conjugates for drug delivery. Chem Mater. 2012;24(5):840–53.
50. Rowinsky EK, Rizzo J, Ochoa L, Takimoto CH, Forouzesh B, Schwartz G, *et al.* A phase I and pharmacokinetic study of pegylated camptothecin as a 1-hour infusion every 3 weeks in patients with advanced solid malignancies. J Clin Oncol. 2003;21(1):148–57.
51. Kainthan RK, Hester SR, Levin E, Devine DV, Brooks DE. In vitro biological evaluation of high molecular weight hyperbranched polyglycerols. Biomaterials. 2007;28(31):4581–90.
52. Pasut G, Scaramuzza S, Schiavon O, Mendichi R, Veronese FM. PEG-epirubicin conjugates with high drug loading. J Bioact Compat Pol. 2005;20(3):213–30.
53. Singer JW. Paclitaxel poliglumex (XYOTAX, CT-2103): a macromolecular taxane. J Control Release. 2005;109(1–3):120–6.
54. Lu ZR. Molecular imaging of HPMA copolymers: visualizing drug delivery in cell, mouse and man. Adv Drug Deliver Rev. 2010;62(2): 246–57.
55. Wang Y, Ye F, Jeong E-K, Sun Y, Parker DL, Lu ZR. Noninvasive visualization of pharmacokinetics, biodistribution and tumor targeting of poly N-(2-hydroxypropyl)methacrylamide

in mice using contrast enhanced MRI. Pharm Res. 2007;24(6):1208–16.
56. Lammers T, Subr V, Peschke P, Kuhnlein P, Hennink WE, Ulbrich K, *et al.* Image-guided and passively tumour-targeted polymeric nanomedicines for radiochemotherapy. Brit J Cancer. 2008;99(6):900–10.
57. Blanco E, Kessinger CW, Sumer BD, Gao J. Multifunctional micellar nanomedicine for cancer therapy. Exp Biol Med (Maywood). 2009;234(2):123–31.
58. Kim TY, Kim DW, Chung JY, Shin SG, Kim SC, Heo DS, *et al.* Phase I and pharmacokinetic study of Genexol-PM, a cremophor-free, polymeric micelle-formulated paclitaxel, in patients with advanced malignancies. Clin Cancer Res. 2004;10(11):3708–16.
59. Lee KS, Chung HC, Im SA, Park YH, Kim CS, Kim SB, *et al.* Multicenter phase II trial of Genexol-PM, a Cremophor-free, polymeric micelle formulation of paclitaxel, in patients with metastatic breast cancer. Breast Cancer Res Tr. 2008;108(2):241–50.
60. Ahmed F, Discher DE. Self-porating polymersomes of PEG-PLA and PEG-PCL: hydrolysis-triggered controlled release vesicles. J Control Release. 2004;96(1):37–53.
61. Sun H, Guo B, Cheng R, Meng F, Liu H, Zhong Z. Biodegradable micelles with sheddable poly(ethylene glycol) shells for triggered intracellular release of doxorubicin. Biomaterials. 2009;30(31):6358–66.
62. Gillies ER, Frechet JMJ. pH-responsive copolymer assemblies for controlled release of doxorubicin. Bioconjugate Chem. 2005;16(2):361–8.
63. Rapoport N. Physical stimuli-responsive polymeric micelles for anti-cancer drug delivery. Prog Polym Sci. 2007;32(8–9):962–90.
64. Xiong J, Meng F, Wang C, Cheng R, Liu Z, Zhong Z. Folate-conjugated crosslinked biodegradable micelles for receptor-mediated delivery of paclitaxel. J Mater Chem. 2011;21(15):5786–94.
65. Kim Y, Pourgholami MH, Morris DL, Stenzel MH. Triggering the fast release of drugs from crosslinked micelles in an acidic environment. J Mater Chem. 2011;21(34):12777–83.
66. Kim Y, Pourgholami MH, Morris DL, Stenzel MH. Effect of cross-linking on the performance of micelles as drug delivery carriers: a cell uptake study. Biomacromolecules. 2012;13(3):814–25.
67. Lee S-Y, Kim S, Tyler JY, Park K, Cheng J-X. Blood-stable, tumor-adaptable disulfide bonded mPEG-$(Cys)_4$-PDLLA micelles for chemotherapy. Biomaterials. 2013;34(2):552–61.
68. Lu J, Ma S, Sun J, Xia C, Liu C, Wang Z, *et al.* Manganese ferrite nanoparticle micellar nanocomposites as MRI contrast agent for liver imaging. Biomaterials. 2009;30(15):2919–28.
69. Liu G, Wang Z, Lu J, Xia C, Gao F, Gong Q, *et al.* Low molecular weight alkyl-polycation wrapped magnetite nanoparticle clusters as MRI probes for stem cell labeling and in vivo imaging. Biomaterials. 2011;32(2):528–37.
70. Su H, Liu Y, Wang D, Wu C, Xia C, Gong Q, *et al.* Amphiphilic starlike dextran wrapped superparamagnetic iron oxide nanoparticle clsuters as effective magnetic resonance imaging probes. Biomaterials. 2013;34(4):1193–203.
71. Wang Z, Liu G, Sun J, Wu B, Gong Q, Song B, *et al.* Self-assembly of magnetite nanocrystals with amphiphilic polyethylenimine: structures and applications in magnetic resonance Imaging. J Nanosci Nanotechno. 2009;9(1):378–85.
72. Hoang B, Lee H, Reilly RM, Allen C. Noninvasive monitoring of the fate of ^{111}In-labeled block copolymer micelles by high resolution and high sensitivity microSPECT/CT imaging. Mol Pharm. 2009;6(2):581–92.
73. Gao X, Cui Y, Levenson RM, Chung LW, Nie S. In vivo cancer targeting and imaging with semiconductor quantum dots. Nat Biotechnol. 2004;22(8):969–76.
74. Bruchez M, Moronne M, Gin P, Weiss S, Alivisatos AP. Semiconductor nanocrystals as fluorescent biological labels. Science. 1998;281(5385):2013–6.
75. Qin SH, Geng Y, Discher DE, Yang S. Temperature-controlled assembly and release from polymer vesicles of poly(ethylene oxide)-block-poly(N-isopropylacrylamide). Adv Mater. 2006;18(21):2905–9.
76. Dubertret B, Skourides P, Norris DJ, Noireaux V, Brivanlou AH, Libchaber A. In vivo imaging of quantum dots encapsulated in phospholipid micelles. Science. 2002;298(5599):1759–62.
77. O'Reilly RK, Joralemon MJ, Wooley KL, Hawker CJ. Functionalization of micelles and shell cross-linked nanoparticles using click chemistry. Chem Mater. 2005;17(24):5976–88.
78. Wang D, Su H, Liu Y, Wu C, Xia C, Sun J, *et al.* Near-infrared fluorescent amphiphilic polycation wrapped magnetite nanoparticles as multimodality probes. Chinese Sci Bull. 2012;57(31):4012–8.
79. Nasongkla N, Bey E, Ren J, Ai H, Khemtong C, Guthi JS, *et al.* Multifunctional polymeric micelles as cancer-targeted, MRI-ultrasensitive drug delivery systems. Nano Lett. 2006;6(11):2427–30.
80. Kessinger CW, Khemtong C, Togao O, Takahashi M, Sumer BD, Gao JM. In vivo angiogenesis imaging of solid tumors by $\alpha_v\beta_3$-targeted, dual-modality micellar nanoprobes. Exp Biol Med (Maywood). 2010;235(8):957–65.
81. AlJamal WT, Kostarelos K. Liposomes: from a clinically established drug delivery system to a nanoparticle platform for theranostic nanomedicine. Accounts Chem Res. 2011;44(10):1094–104.
82. Harris L, Batist G, Belt R, Rovira D, Navari R, Azarnia N, *et al.* Liposome-encapsulated doxorubicin compared with conventional doxorubicin in a randomized multicenter trial as first-line therapy of metastatic breast carcinoma. Cancer. 2002;94(1):25–36.
83. Torchilin VP. Recent advances with liposomes as pharmaceutical carriers. Nat Rev Drug Discov. 2005;4(2):145–60.
84. Lindner LH, Hossann M. Factors affecting drug release from liposomes. Curr Opin Drug Disc. 2010;13(1):111–23.
85. Wang HJ, Wang S, Liao ZY, Zhao PQ, Su WY, Niu RF, *et al.* Folate-targeting magnetic core-shell nanocarriers for selective drug release and imaging. Int J Pharmaceut. 2012;430(1–2):342–9.
86. Mylonopoulou E, Arvanitis CD, Bazan-Peregrino M, Arora M, Coussios CC. Ultrasonic activation of thermally sensitive liposomes. 9th International Symposium on Therapeutic Ultrasound. 2010;1215: 83–87
87. Mitchell N, Kalber TL, Cooper MS, Sunassee K, Chalker SL, Shaw KP, *et al.* Incorporation of paramagnetic, fluorescent and PET/SPECT contrast agents into liposomes for multimodal imaging. Biomaterials. 2013;34(4):1179–92.
88. Kenny GD, Kamaly N, Kalber TL, Brody LP, Sahuri M, Shamsaei E, *et al.* Novel multifunctional nanoparticle mediates siRNA tumour delivery, visualisation and therapeutic tumour reduction *in vivo*. J Control Release. 2011;149(2):111–6.
89. Petersen AL, Binderup T, Jolck RI, Rasmussen P, Henriksen JR, Pfeifer AK, *et al.* Positron emission tomography evaluation of somatostatin receptor targeted ^{64}Cu-TATE-liposomes in a human neuroendocrine carcinoma mouse model. J Control Release. 2012;160(2):254–63.
90. Na K, Lee SA, Jung SH, Shin BC. Gadolinium-based cancer therapeutic liposomes for chemotherapeutics and diagnostics. Colloid and Surface B. 2011;84(1):82–7.
91. Fattahi H, Laurent S, Liu F, Arsalani N, Elst LV, Muller RN. Magnetoliposomes as multimodal contrast agents for molecular imaging and cancer nanotheragnostics. Nanomedicine. 2011;6(3):529–44.
92. Pradhan P, Giri J, Rieken F, Koch C, Mykhaylyk O, Doblinger M, *et al.* Targeted temperature sensitive magnetic liposomes for thermo-chemotherapy. J Control Release. 2010;142(1):108–21.
93. Lo S-T, Kumar A, Hsieh J-T, Sun X. Dendrimer nanoscaffolds for potential theranostics of prostate cancer with a focus on radiochemistry. Mol Pharm. 2013;10(3):793–812.
94. Boas U, Heegaard PMH. Dendrimers in drug research. Chem Soc Rev. 2004;33(1):43–63.

95. Mintzer MA, Grinstaff MW. Biomedical applications of dendrimers: a tutorial. Chem Soc Rev. 2011;40(1):173–90.
96. Thomas TP, Huang BH, Choi SK, Silpe JE, Kotlyar A, Desai AM, *et al.* Polyvalent dendrimer-methotrexate as a folate receptor-targeted cancer therapeutic. Mol Pharm. 2012;9(9):2669–76.
97. Luo K, Liu G, She W, Wang Q, Wang G, He B, *et al.* Gadolinium-labeled peptide dendrimers with controlled structures as potential magnetic resonance imaging contrast agents. Biomaterials. 2011;32(31):7951–60.
98. Luo K, Liu G, He B, Wu Y, Gong Q, Song B, *et al.* Multifunctional gadolinium-based dendritic macromolecules as liver targeting imaging probes. Biomaterials. 2011;32(10):2575–85.
99. Xie J, Xu C, Kohler N, Hou Y, Sun S. Controlled PEGylation of monodisperse Fe_3O_4 nanoparticles for reduced non-specific uptake by macrophage cells. Adv Mater. 2007;19(20):3163–6.
100. Jun YW, Huh YM, Choi JS, Lee JH, Song HT, Kim S, *et al.* Nanoscale size effect of magnetic nanocrystals and their utilization for cancer diagnosis via magnetic resonance imaging. J Am Chem Soc. 2005;127(16):5732–3.
101. Zhao Y, Li Y, Song Y, Jiang W, Wu Z, Wang YA, *et al.* Architecture of stable and water-soluble CdSe/ZnS core-shell dendron nanocrystals via ligand exchange. J Colloid Interface Sci. 2009;339(2):336–43.
102. Chang Y, Meng X, Zhao Y, Li K, Zhao B, Zhu M, *et al.* Novel water-soluble and pH-responsive anticancer drug nanocarriers: doxorubicin-PAMAM dendrimer conjugates attached to superparamagnetic iron oxide nanoparticles (IONPs). J Colloid Interface Sci. 2011;363(1):403–9.
103. Wen SH, Li KG, Cai HD, Chen Q, Shen MW, Huang YP, *et al.* Multifunctional dendrimer-entrapped gold nanoparticles for dual mode CT/MR imaging applications. Biomaterials. 2013;34(5):1570–80.
104. Criscione JM, Dobrucki LW, Zhuang ZW, Papademetris X, Simons M, Sinusas AJ, *et al.* Development and application of a multimodal contrast agent for SPECT/CT hybrid imaging. Bioconjugate Chem. 2011;22(9):1784–92.
105. Pan BF, Cui DX, Sheng Y, Ozkan CG, Gao F, He R, *et al.* Dendrimer-modified magnetic nanoparticles enhance efficiency of gene delivery system. Cancer Res. 2007;67(17):8156–63.
106. Merkel OM, Mintzer MA, Librizzi D, Samsonova O, Dicke T, Sproat B, *et al.* Triazine dendrimers as nonviral vectors for in vitro and in vivo RNAi: the effects of peripheral groups and core structure on biological activity. Mol Pharm. 2010;7(4):969–83.
107. Yu TZ, Liu XX, Bolcato-Bellemin AL, Wang Y, Liu C, Erbacher P, *et al.* An amphiphilic dendrimer for effective delivery of small interfering RNA and gene silencing in vitro and in vivo. Angewandte Chemie-International Edition. 2012;51(34):8478–84.
108. Duncan R, Izzo L. Dendrimer biocompatibility and toxicity. Adv Drug Deliv Rev. 2005;57(15):2215–37.
109. Boyle P, Levin, B. World Cancer Report. World Health Organization Press. 2008.
110. Portney NG, Ozkan M. Nano-oncology: drug delivery, imaging, and sensing. Anal Bioanal Chem. 2006;384(3):620–30.
111. Sinha R, Kim GJ, Nie S, Shin DM. Nanotechnology in cancer therapeutics: bioconjugated nanoparticles for drug delivery. Mol Cancer Ther. 2006;5(8):1909–17.
112. Gong J, Chen MW, Zheng Y, Wang SP, Wang YT. Polymeric micelles drug delivery system in oncology. J Control Release. 2012;159(3):312–23.
113. Xiao Y, Hong H, Javadi A, Engle JW, Xu W, Yang Y, *et al.* Multifunctional unimolecular micelles for cancer-targeted drug delivery and positron emission tomography imaging. Biomaterials. 2012;33(11):3071–82.
114. Viglianti BL, Abraham SA, Michelich CR, Yarmolenko PS, MacFall JR, Bally MB, *et al.* In vivo monitoring of tissue pharmacokinetics of liposome/drug using MRI: illustration of targeted delivery. Magn Reson Med. 2004;51(6):1153–62.
115. de Smet M, Heijman E, Langereis S, Hijnen NM, Grull H. Magnetic resonance imaging of high intensity focused ultrasound mediated drug delivery from temperature-sensitive liposomes: an in vivo proof-of-concept study. J Control Release. 2011;150(1):102–10.
116. Negussie AH, Yarmolenko PS, Partanen A, Ranjan A, Jacobs G, Woods D, *et al.* Formulation and characterisation of magnetic resonance imageable thermally sensitive liposomes for use with magnetic resonance-guided high intensity focused ultrasound. Int J Hyperther. 2011;27(2):140–55.
117. Kato Y, Artemov D. Monitoring of release of cargo from nanocarriers by MRI/MR spectroscopy (MRS): significance of T_2/T_2^* effect of iron particles. Magn Reson Med. 2009;61(5):1059–65.
118. Lammers T, Aime S, Hennink WE, Storm G, Kiessling F. Theranostic nanomedicine. Accounts Chem Res. 2011;44(10):1029–38.
119. Onuki Y, Jacobs I, Artemov D, Kato Y. Noninvasive visualization of in vivo release and intratumoral distribution of surrogate MR contrast agent using the dual MR contrast technique. Biomaterials. 2010;31(27):7132–8.
120. Tagami T, Foltz WD, Ernsting MJ, Lee CM, Tannock IF, May JP, *et al.* MRI monitoring of intratumoral drug delivery and prediction of the therapeutic effect with a multifunctional thermosensitive liposome. Biomaterials. 2011;32(27):6570–8.
121. Hanahan D, Weinberg RA. The hallmarks of cancer. Cell. 2000;100(1):57–70.
122. Therasse P, Arbuck SG, Eisenhauer EA, Wanders J, Kaplan RS, Rubinstein L, *et al.* New guidelines to evaluate the response to treatment in solid tumors. J Natl Cancer Inst. 2000;92(3):205–16.
123. Kaida S, Cabral H, Kumagai M, Kishimura A, Terada Y, Sekino M, *et al.* Visible drug delivery by supramolecular nanocarriers directing to single-platformed diagnosis and therapy of pancreatic tumor model. Cancer Res. 2010;70(18):7031–41.
124. Phillips WT, Goins B, Bao A, Vargas D, Guttierez JE, Trevino A, *et al.* Rhenium-186 liposomes as convection-enhanced nanoparticle brachytherapy for treatment of glioblastoma. Neuro-Oncology. 2012;14(4):416–25.
125. Folkman J. Tumor angiogenesis: therapeutic implications. New Engl J Med. 1971;285(21):1182–6.
126. Weidner N, Semple JP, Welch WR, Folkman J. Tumor angiogenesis and metastasis–correlation in invasive breast carcinoma. New Engl J Med. 1991;324(1):1–8.
127. Carmeliet P. Angiogenesis in life, disease and medicine. Nature. 2005;438(7070):932–6.
128. Tozer GM, Kanthou C, Baguley BC. Disrupting tumour blood vessels. Nat Rev Cancer. 2005;5(6):423–35.
129. Underiner TL, Ruggeri B, Gingrich DE. Development of vascular endothelial growth factor receptor (VEGFR) kinase inhibitors as anti-angiogenic agents in cancer therapy. Curr Med Chem. 2004;11(6):731–45.
130. Zhang F, Huang X, Zhu L, Guo N, Niu G, Swierczewska M, *et al.* Noninvasive monitoring of orthotopic glioblastoma therapy response using RGD-conjugated iron oxide nanoparticles. Biomaterials. 2012;33(21):5414–22.
131. Liu G, Xie J, Zhang F, Wang Z, Luo K, Zhu L, *et al.* N-Alkyl-PEI-functionalized iron oxide nanoclusters for efficient siRNA delivery. Small. 2011;7(19):2742–9.
132. Roger VL, Go AS, Lloyd-Jones DM, Adams RJ, Berry JD, Brown TM, *et al.* Update a report from the American Heart Association. Circulation. 2011;123(4):E18–E209.
133. Shaw SY. Molecular imaging in cardiovascular disease: targets and opportunities. Nat Rev Cardiology. 2009;6(9):569–79.

134. Chen IY, Wu JC. Cardiovascular molecular imaging: focus on clinical translation. Circulation. 2011;123(4):425–43.
135. McCarthy JR. Multifunctional agents for concurrent imaging and therapy in cardiovascular disease. Adv Drug Deliver Rev. 2010;62(11):1023–30.
136. Bowey K, Tanguay J-F, Tabrizian M. Liposome technology for cardiovascular disease treatment and diagnosis. Expert Opin Drug Del. 2012;9(2):249–65.
137. Saam T, Hatsukami TS, Takaya N, Chu B, Underhill H, Kerwin WS, *et al.* The vulnerable, or high-risk, atherosclerotic plaque: noninvasive MR imaging for characterization and assessment. Radiology. 2007;244(1):64–77.
138. Jeziorska M, Woolley DE. Neovascularization in early atherosclerotic lesions of human carotid arteries: its potential contribution to plaque development. Hum Pathol. 1999;30(8):919–25.
139. Moreno PR, Purushothaman R, Fuster V, Echeverri D, Truszczynska H, Sharma SK, *et al.* Plaque neovascularization is increased in ruptured atherosclerotic lesions of human aorta: Implications for plaque vulnerability. Circulation. 2004;110(14): 2032–8.
140. Mofidi R, Crotty TB, McCarthy P, Sheehan SJ, Mehigan D, Keaveny TV. Association between plaque instability, angiogenesis and symptomatic carotid occlusive disease. Bri J Surg. 2001;88(7): 945–50.
141. Kolodgie FD, Gold HK, Burke AP, Fowler DR, Kruth HS, Weber DK, *et al.* Intraplaque hemorrhage and progression of coronary atheroma. New Engl J Med. 2003;349(24):2316–25.
142. Winter PM, Neubauer AM, Caruthers SD, Harris TD, Robertson JD, Williams TA, *et al.* Endothelial $\alpha_v\beta_3$ integrin-targeted fumagillin nanoparticles inhibit angiogenesis in atherosclerosis. Arterioscl Throm Vas. 2006;26(9):2103–9.
143. Libby P. Inflammation in atherosclerosis. Nature. 2002;420(6917): 868–74.
144. Jaffer FA, Libby P, Weissleder R. Molecular imaging of cardiovascular disease. Circulation. 2007;116(9):1052–61.
145. Lobatto ME, Fayad ZA, Silvera S, Vucic E, Calcagno C, Mani V, *et al.* Multimodal clinical imaging to longitudinally assess a nanomedical anti-inflammatory treatment in experimental atherosclerosis. Mol Pharm. 2010;7(6):2020–9.
146. Moses JW, Leon MB, Popma JJ, Fitzgerald PJ, Holmes DR, O'Shaughnessy C, *et al.* Sirolimus-eluting stents versus standard stents in patients with stenosis in a native coronary artery. New Engl J Med. 2003;349(14):1315–23.
147. Braun RM, Cheng J, Parsonage EE, Moeller J, Winograd N. Surface and depth profiling investigation of a drug-loaded copolymer utilized to coat Taxus Express(2) stents. Anal Chem. 2006;78(24):8347–53.
148. Lanza GM, Yu X, Winter PM, Abendschein DR, Karukstis KK, Scott MJ, *et al.* Targeted antiproliferative drug delivery to vascular smooth muscle cells with a magnetic resonance imaging nanoparticle contrast agent implications for rational therapy of restenosis. Circulation. 2002;106(22):2842–7.
149. Tran TD, Caruthers SD, Hughes M, Marsh JN, Cyrus T, Winter PM, *et al.* Clinical applications of perfluorocarbon nanoparticles for molecular imaging and targeted therapeutics. Int J Nanomed. 2007;2(4):515–26.
150. Myerson J, He L, Lanza G, Tollefsen D, Wickline S. Thrombin-inhibiting perfluorocarbon nanoparticles provide a novel strategy for the treatment and magnetic resonance imaging of acute thrombosis. J Thromb Haemost. 2011;9(7):1292–300.
151. Cyrus T, Zhang H, Allen JS, Williams TA, Hu G, Caruthers SD, *et al.* Intramural delivery of rapamycin with $\alpha_v\beta_3$-targeted paramagnetic nanoparticles inhibits stenosis after balloon injury. Arterioscl Throm Vas. 2008;28(5):820–6.
152. Park K. Facing the truth about nanotechnology in drug delivery. ACS Nano. 2013;7(9):7442–7.